CHAPTER V
SYNTHESIS, MODIFICATION, AND CHARACTERIZATION OF SILVER NANOPARTICLE LOADED BENTONITE

5.1   Abstract

A silver nanoparticles-filled clay is aimed to be an antimicrobial agent in the nanocomposite films in the Chapter VII. This section presents the synthesis of silver nanoparticles into the interlayer of nanoclay through a green approach by varying the weight percentages of silver nanoparticles (5, 10, 15, and 20 wt%) to study the effect of nanoparticle contents on antimicrobial activities of nanocomposite films in the Chapter VII. Silver nitrate acts as a precursor, whereas sodium citrate does as a reducing agent. Silver nanoparticle-loaded bentonites (SBEN) were then modified with γ-methacryloxypropyltrimethoxysilane (γ-MPS), so called modified silver nanoparticle-loaded bentonites (MSBEN) prior to mixing with polypropylene via a reactive extrusion in the next chapter. TEM analysis asserted a high density of spherical silver nanoparicles with a particle size of 30 nm in average. XRD patterns showed the intercalation of silver nanoparticles in the intergalleries of bentonite. The four crystal planes of face-centered cubic silver nanoparticles appeared at approximately 38, 44, 64, and 77 degrees of two-theta angles corresponding to (111), (200), (220), and (311), respectively. Clearly, all the crystallographic planes due to the existence of silver nanoparticles were found to augment along with the content of silver. Moreover, the organosilane introduced within the SBEN was achieved after modification of the SBEN with γ-MPS. The absorption bands at 2917 and 2851 cm^{-1} were due to the stretching vibrations of CH bonds. The spectra appeared at 1717 and 1641 cm^{-1} agreeing with stretching vibrations of C=O and C=C groups, respectively as well as the peaks approximately 1000 cm^{-1} were associated with bending vibrations of Si-O-C bonds.

Keywords: Bentonite, γ-Methacryloxypropyltrimethoxysilane, Silver nanoparticles

5.2 Introduction

With the advent of antimicrobial packaging, the incorporation of antimicrobial agents show promise as an effective way for the resistance of certain microorganisms in foods (Cooksey, 2005). Among metallic nanoparticles, silver nanoparticles manifest its wide ranges of application in various sections of life and industry. The silver is an effective antibacterial metal and non-toxic to animal cells but strongly toxic to bacteria, such as *Escherchia coli* (*E. coli*) (Ghosh and Ramamoorthy, 2010) and *Staphylococcus aureas* (El-Kheshen and Gad El-Rab, 2012), as well as highly toxic against fungi, such as *Candida albicans* (*C. albicans*), *Saccharomyces cerevisiae* (*S. cerevisiae*) (Nasrollahi *et al.*, 2011), and *Colletotrichum* species (Lamdal *et al.*, 2011). Silver nanoparticles, in particular, have exhibited extraordinary properties for antimicrobial agents in food packaging. For silver nanoparticles are able to disrupt enzymatic activity of microbial cells, one important purpose of addition of these metallic silver nanoparticles is to prolong the shelf-life and boost the safety of meat products by diminishing the rate of surface growth of specific microorganisms by direct contact of the packaging with the products (Appendini and Hotchkiss, 2002).

This chapter involves the synthesis and modification of silver nanoparticle – loaded clay and includes its characterizations. The purpose of incorporation of silver nanoparticles in the bentonite is to enhance the antimicrobial activities of PP nanocomposite films for fish packaging. This study presents the synthesis of silver nanoparticles – loaded bentonite (SBEN) via a one – step method based on an environmental – friendly chemical reduction adapted from Gorup *et al.* (2009), El-Kheshen and Gad El-Rab (2012) and Shameli *et al.* (2011). The silver ions were loaded onto various inorganic carriers by an ion-exchange method, followed by a chemical reduction step. Silver nitrate acted as a precursor, while sodium citrate functioned as a reducing agent. Contents of silver nanoparticles were applied at various concentrations of 5, 10, 15, and 20 wt% within the clay layers so that we would determine their effects on antibacterial activites at different amounts of metal nanoparticles in the Chapter VII. The characterizations of SBEN were studied by means of transmission electron microscopy (TEM) and X-ray diffraction (XRD)

techniques. Concurrently, FTIR spectra affirmed the successful modification of SBEN.

5.3   Experimental Procedures

5.3.1   Materials

The commercial sodium activated bentonite Mac-Gel® (GRADE SAC), Na-BTN, with cationic exchange capacity (CEC) of 49.74 meq/100 g clay and surface area of 31.0 m^2/g, supplied by Thai Nippon Chemical Industry Co., Ltd., Thailand, was purified before use. Silver (I) nitrate ($AgNO_3$), CAS NO. 7761-88-8, was purchased from Carlo Erba and used as received. Trisodium citrate dihydrate ($Na_3C_6H_5O_7$), CAS NO. 6132-04-3, was purchased from Carlo Erba and used as received. Absolute ethanol (C_2H_5OH), AR grade, CAS NO. 64-17-5, and glacial acetic acid (CH_3COOH), CAS NO. 64-19-7, were purchased from RCI Labscan and used as received, respectively.

5.3.2   Preparation of Purified Clay

The sodium bentonite clay was first vigorously stirred into an alkaline water (pH 9) at 700 rpm overnight by a mechanical stirrer. After that, the supernatant (swollen clay) was separated by centrifugation at 10,000 rpm for 15 minutes and lastly dried, sieved by mesh#400 and kept in a dessiccator before use.

5.3.3   Synthesis of Silver Nanoparticles into the Interlayer Space of Clay

50 g of bentonite were firstly stirred in $AgNO_3$ solution at room temperature overnight. The silver clay was then reacted with $C_6H_5Na_3O_7 2H_2O$ at 1 : 3 molar ratio of $AgNO_3$ to $C_6H_5Na_3O_7 2H_2O$ at 90 °C for 20 min to obtain silver nanoparticles - loaded clay (SBEN). The as-synthesized silver nanoparticles clay was measured their shape and size by a transmission electron microscope (TEM) as well as their crystal structure by an X-ray diffractometer (XRD).

5.3.4   Modification of Silver Nanoparticles-Loaded Clay (SBEN)

The method was adapted from Chaijareenont *et al.* (2012) and Marquez *et al.* (2005). 1.5 wt.% of MPS solution was prepared in 70 vol.% of ethanol aqueous solution pH 4 adjusted by glacial acetic acid and then stirred for 45 min of hydrolysis to silanol. 50 g of SBEN were added respectively into the MPS

solution. The mixture was stirred at 110 °C for 24 hours. The plenty of absolute ethanol was used for the removal of excessive MPS during suction filtrating and the modified silver nanoparticles-loaded bentonite (MSBEN) was finally dried at 80 °C in a vacuum oven for 24 hrs. The MSBEN was sieved by mesh#400 and kept in a desiccator prior to use.

5.3.5 Characterizations

5.3.5.1 Transmission Electron Microscope (TEM)

Transmission electron microscopy of synthesized silver nanoparticles was performed on JEOL JEM-2100 model and at accelerating voltage of 200 kV. Samples for TEM imaging were prepared by placing a drop of the colloidal solution of each type of clay on a copper grid.

5.3.5.2 X-ray Diffractometer (XRD)

The crystal structure of bentonite and silver nanoparticles in bentonite was analyzed by wide angle X-ray diffraction (WAXD) using a Bruker AXS model Diffractrometer D8with Ni-filtered Cu K_α radiation operated at 40 kV and 30 mA. The experiment was performed in the 2θ range of 5 – 80 degrees with scan speed 2 degree/min and scan step 0.01 degree.

5.3.5.3 Fourier Transform Infared Spectrometer (FT-IR)

The FT-IR spectra of BEN, SBEN, and MSBEN were collected by using a Nicolet Nexus 670 FT-IR spectrometer over a wave number range of 4,000 – 400 cm^{-1} with 64 scans at a resolution of 4 cm^{-1}.

5.4 Results and Discussion

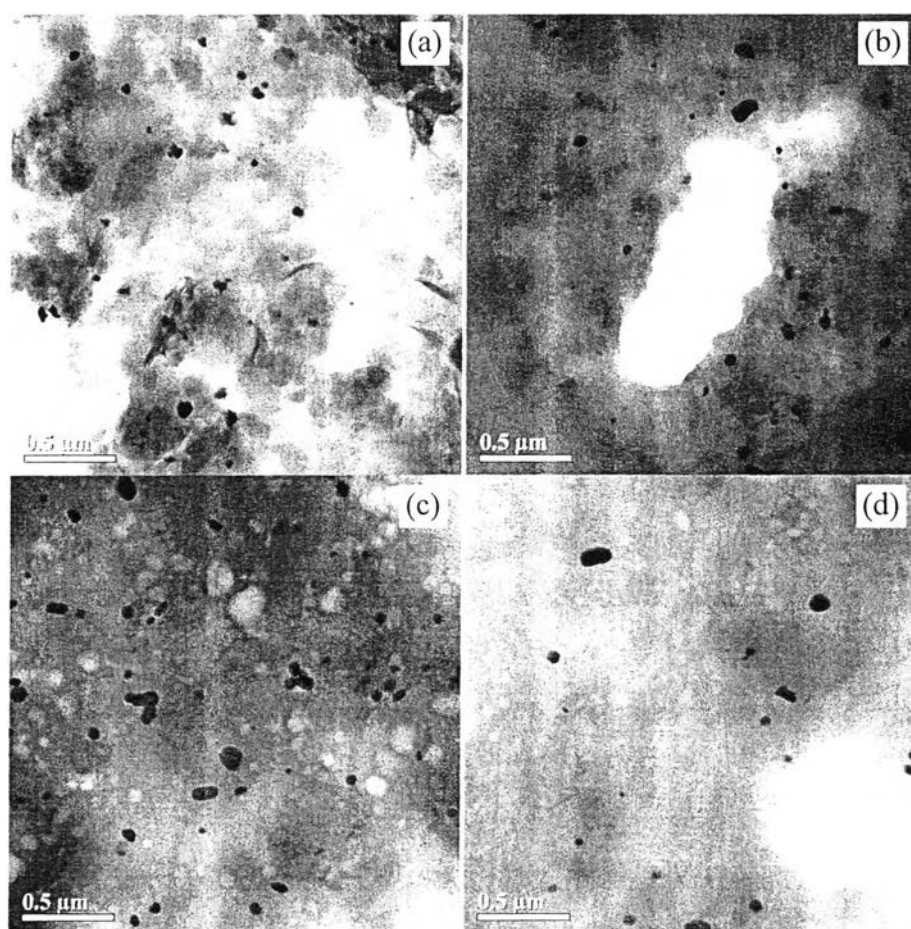### 5.4.1 Characterization of Silver Nanoparticle-Loaded Bentonite by a TEM

Figure 5.1 TEM images of silver nanoparticles-loaded bentonite (SBEN) at (a) 5, (b) 10, (c) 15, and (d) 20 wt% of metal nanoparticles.

During the chemical reduction method, silver ions was reduced by a portion of the sodium citrate at high pH and elevated temperature, while the remaining citrate was able to cap and protected the particles from aggregation. The sodium citrate donated electrons to the silver ions (Ag^+), resulting in the metallic form of silver (Ag^0), proposed by the mechanism as follows (El-Kheshen and Gad El-Rab, 2012; Augustin and Rajarathinam, 2012):

$$4Ag^+ + C_6H_5O_7Na_3 + 2H_2O \longrightarrow 4Ag^0 + C_6H_5O_7H_3 + 3Na^+ + H^+ + O_2 \uparrow \quad \text{(Eq. 5.1)}$$
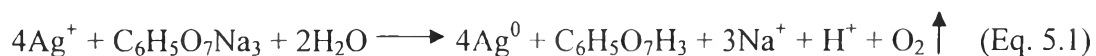
Figure 5.1 shows TEM images of silver nanoparticles synthesized via the chemical reduction method reported by Gorup *et al.* (2009), El-Kheshen and Gad El-Rab (2012) and Shameli *et al.* (2011). The size distribution was reported around 30 nm in average. The spherical shape of silver nanoparticles was presented in these images but some aggregates were formed. However, Gorup *et al.* (2009) reported that it was difficult to propose a simple kinetic model for the growth of silver nanoparticles because there were several variables to consider, such as the cleanliness of glasswares, the purity of water and reagents, solution temperature, concentrations of metal salt and reducing agent and also reaction time (Kheshen and Gad El-Rab, 2012). For example, the density of nuclei and reaction time may interdependently serve to shed light on the formation of these monodisperse nanoparticles with small sizes (Gorup *et al.*, 2009).

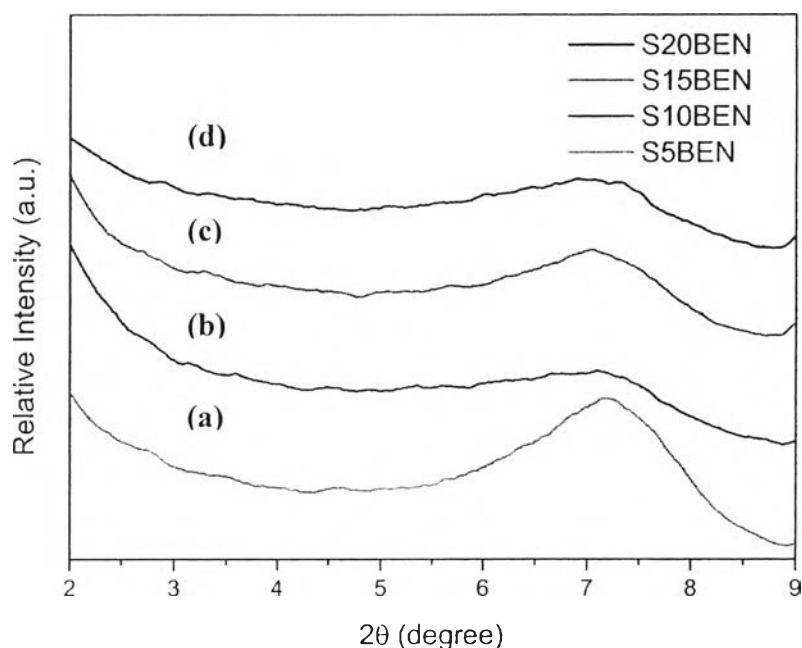5.4.2 Investigation of the Crystal Structure of Silver Nanoparticle-Loaded Bentonite by an XRD

Figure 5.2 SAXD patterns at small angle of silver nanoparticles-loaded bentonite (SBEN) at (a) 5, (b) 10, (c) 15, and (d) 20 wt% of these nanoparticles.

Table 5.1 2-theta value and d-spacing of bentonite after the incorporation of silver nanoparticles at different weight percentages of these nanoparticles

Sample	2-theta (deg)	d-spacing (Å)
BEN	7.34	12.0
S5BEN	7.20	12.3
S10BEN	7.10	12.5
S15BEN	7.00	12.6
S20BEN	6.92	12.8

According to the figure 5.3 and the table 5.1, XRD patterns showed a little shift of 2-theta of (001) plane of bentonite to lower degree after higher amount of silver nanoparticles was synthesized in the bentonite. Based on the Bragg's law, the lowering 2-theta was about an increase in d-spacing of interlayers of bentonite. The original d-spacing of pristine clay (12.0 Å at 2-theta angle of 7.30 degree) was increased to 12..3, 12.5, 12.6, and finally 12.8 Å at the 2-thata angles of 7.20, 7.10, 7.00, and 6.92 degrees, respectively. At 20 wt% of silver nanoparticles added, the d-spacing was obviously higher around 0.8 Å compared to that of pristine clay. Therefore, a slight increase in d-spacing took place along with a degree of intercalation of silver nanoparticles in the interlamellar spaces of bentonite. For all the samples, their half-widths of (001) were vividly greater than that of pristine clay, in which the metallic silver nanoparticles disrupted the highly-ordered lamellar structure of clay in consonance with Shameli *et al.*'s research (2010 and 2011). They found that the interlayer spaces of montmorillonite were changed to increase along with the high amount of silver nanoparticles synthesized into their interlayer. The silver nanoparticles formed located on not only the internal surface, but also the external surface of clay. Furthermore, the ordered structure of montmorillonite was distorted because of the addition of spherical silver nanoparticles.
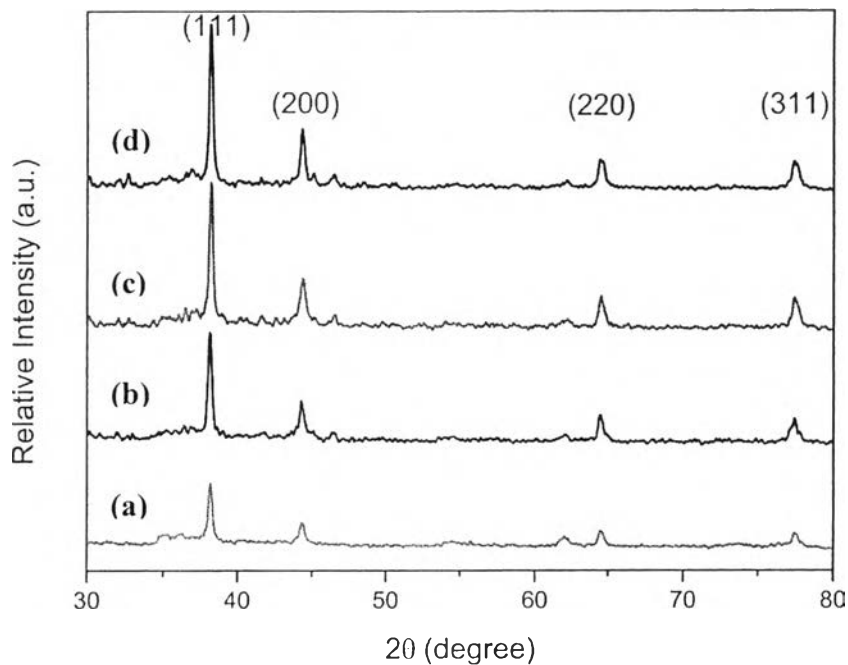
Figure 5.3 WAXD patterns at small angle of silver nanoparticles-loaded bentonite (SBEN) at (a) 5, (b) 10, (c) 15, and (d) 20 wt% of these nanoparticles.

In the wide angle range of 2-theta (Figure 5.3), XRD patterns showed four crystallographic planes of silver nanoparticles appeared at 38.36°, 44.48°, 64.66°, and 77.42° of two-theta angles corresponding to (111), (200), (220), and (311), attributed to the face-centered cubic silver crystals, respectively. The major crystalline phase was silver for all of the samples, whereas no evident phases of impurities were found in the XRD patterns. Clearly, all of the four crystallographic planes of (111), (200), (220), and (311) owing to the existence of silver nanoparticles were found to increase together with the content of silver.

5.4.3 FTIR Spectra of Silver Nanoparticles-Loaded Bentonite (SBEN)

In order to confirm the attachment of citrate molecules with the silver nanoparticles, the spectra of SBEN are run as shown in the Figure 5.4 in comparison to the spectra of bentonite and sodium citrate crystal. For all the S15BEN and S20BEN, the weak peaks at 2961 and 2917 cm^{-1} were assigned to the stretching vibrations of hydrocarbon from the sodium citrate (reducing agent), yet these peaks

were very weak to be observed in the case of S5BEN and S10BEN, resulting from a few amount of sodium citrate added. Nevertheless, for all SBENs, they did not show the sharp peak at 1654 cm^{-1} of $AgNO_3$, which was due to the loss of nitrate groups from the silver species, suggesting that they exhibited the FTIR spectra of silver nanoparticles synthesized in the nanoclay, according to the data report from Augustin and Rajarathinam (2012). Regarding the FTIR spectrum of the sodium citrate crystal, the band at 3453 cm^{-1} was assigned to the stretching vibration of –OH, the band at 1589 cm^{-1} was related to the asymmetric stretching of –COO, and at 1417 cm^{-1} was attributed to the symmetric stretching of –COO group. After silver nanoparticles were synthesized by using the sodium citrate as a reducing agent, the asymmetric band at 1589 cm^{-1} of the citrate were still the same position of this band of all the SBENs, at around 1597 cm^{-1}. However, it was clearly shown that the redshift of 1417 cm^{-1} of the citrate to 1389 cm^{-1} of the SBENs accounted for the formation of metal-bound –COO group. This is due to the stabilization of –COO group from the sodium citrate. This shift can be comparable with the previous works from Anupam Giri *et al.* (2010). They speculated that when the citrate ligand bound to the surfaces of magnetite nanoparticles the asymmetric –COO stretching at 1595 cm^{-1} remained unchanged, yet the the symmetric –COO stretching of the citrate went redshifted to sharply appear at 1398 cm^{-1}. Moreover, they added that the main interacting species that can interact with the ligand was the nanoparticles because they observed that the –OH stretching vibration of the citrate remained intact and was significantly broaden after it interacted with these nanoparticles consistent with the result in the Figure 5.4. To sum up, in addition to this reducing function, the citrate was capped on the surface of these nanoparticles as a stabilizer for preventing the propagation and agglomeration (Augustin and Rajarathinam, 2012).
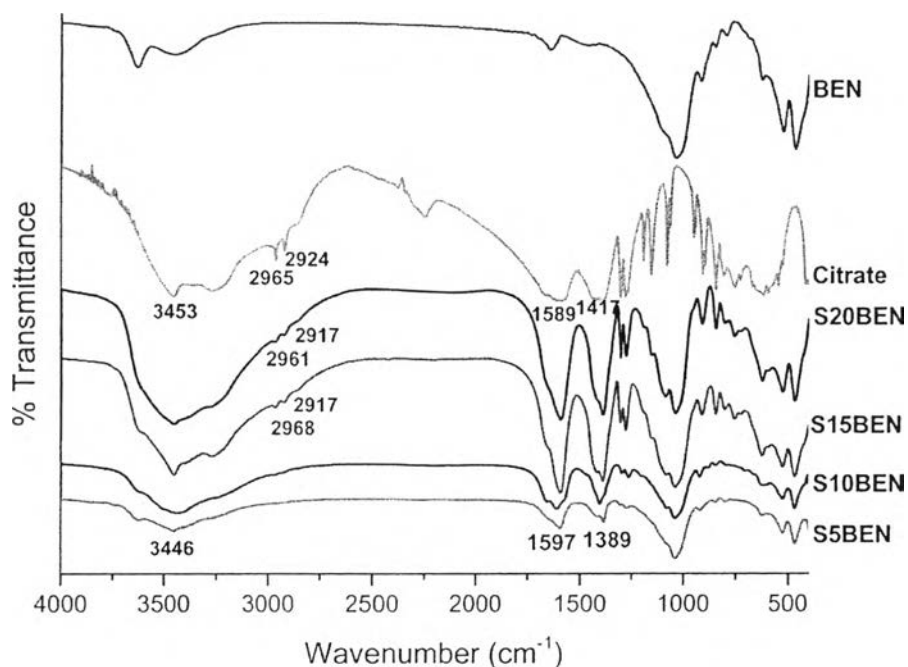
Figure 5.4 FTIR spectra of pristine bentonite, sodium citrate, and silver nanoparticles-loaded bentonite at various contents of silver nanoparticles (SBEN).

5.4.4 FTIR Spectra of γ-MPS-Modified Silver Nanoparticles-Loaded Bentonite (MSBEN)

The spectra of MSBEN are illustrated in the Figure 5.4. The figure showed a strong band around 3400 cm^{-1} corresponding to trapped water molecules (Maria *et al.*, 2011, Rodriguez *et al.*, 1999). The medium sharp band at 920 and 845 cm^{-1} were assigned to Al-Al-OH and Al-Mg-OH bonds, respectively (Żymankowska-kumon *et al.*, 2012). The absorption bands at 620 and 524 cm^{-1} were due to Al–O–Si bending vibrations (Żymankowska-kumon *et al.*, 2012), as well as the sharp band at 467 cm^{-1} was attributed to Si–O–Si bending vibrations (Zhirong *et al.*, 2011). The very strong absorption band at 1041 cm^{-1} was due to Si–O bending vibration (Rodriguez *et al.*, 1999).
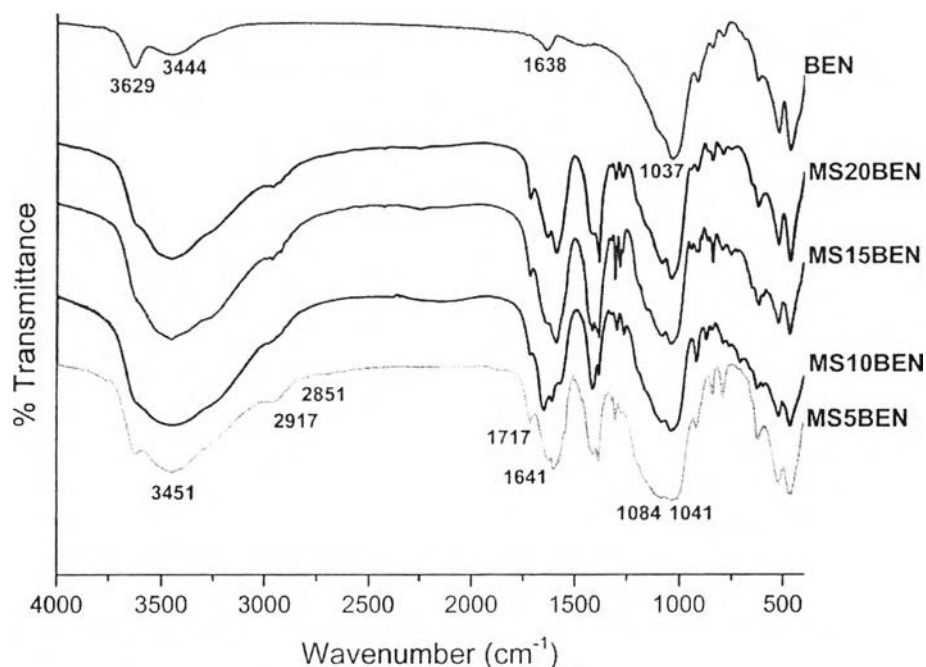
Figure 5.5   FTIR spectra of modified silver nanoparticle-loaded bentonite at different contents of silver nanoparticles (MSBEN).

After the silylation is completed, all of the MSBENs showed new spectra bands at which the grafting of the organosilane was formed. The weak absorption signals at 2917 and 2851 cm^{-1} were because of the stretching vibrations of aliphatic hydrocarbon (CH bonds; CH_3 and CH_2), thus confirming the organic moieties on the clay surface (Maria *et al.*, 2011, Rodriguez *et al.*, 1999, Zhirong *et al.*, 2011). The new bands at 1717 and 1641 cm^{-1} were associated with the stretching vibrations of C=O and C=C groups, respectively as well as the peaks around 1000 cm^{-1} were concerned with bending vibrations of Si-O-C bonds (Rodriguez *et al.*, 1999). Moreover, compared to all the SBENs' spectra, it was worth noting that the increasing relative intensities of the peaks at 3451 cm^{-1} corresponding to –OH stretching of certain dimers/oligomers of uncondensed hydroxyl silane molecules (silanols) at the edge of the clay layer (Vrancken *et al.*, 1995). The similar notice was in compliance with the FTIR spectrum of MBEN compared to BEN in the former chapter. This remark was reported by Antonucci *et al.*, (2005), they commented that the broad band with the peak at 3450 cm^{-1} were primarily ascribed to OH stretching

of Si—OH plausibly bonded to O=C groups, or may result from Si—OH hydrogen bonded to other Si—OH groups and from water hydrogen bonded to itself and to the Si—OH groups. Concurrently, peaks in the range of 1100-1000 cm^{-1} involved in the Si—O—Si stretching of MSBENs become progressively more pronounced compared to SBENs and BEN, suggesting the presence of a higher amount of intercalated and/or grafted silane modifiers (Piscitelli *et al.*, 2010).

5.5 Conclusions

Silver nanoparticles – loaded bentonite (SBEN) was synthesized via a green chemical reduction method without any inert gas protection. TEM analysis reported the average size of 30 nm in spherical shape of silver nanoparticles. For their crystal structure, XRD Patterns confirmed the formation of pure silver nanoparticles and demonstrated their crystallographic planes of face-centered cubic silver nanoparticles. XRD, moreover, revealed the change in (001) plane of bentonite owing to the slight intercalation of metallic nanoparticles in the clay galleries. Finally, the modified silver nanoparticle–loaded bentonite (MSBEN) was successfully obtained via the modification of SBEN with the organosilane, insisted by the stretching vibrations of CH bonds, C=O, and C=C groups including the bending vibrations of Si-O-C bonds.

5.6 Acknowledgements

5.7 References

Antonucci, J. M., Dickens, S. H., Fowler, B. O., Xu, H. H. K.,. McDonough, W. G. (2005) Chemistry of Silanes: Interfaces in Dental Polymers and Composites. Journal of Research of National Institute of Standards and Technology, 110, 541-558.

Appendini, P., Hotchkiss, J.H. (2002) Review of Antimicrobial Food Packaging. Innovative Food Science & Emerging Technologies, 3, 113-126.

Augustin, R., Rajarathinam, K. (2012) Synthesis and Characterization of Silver Nanoparticles and its Immobilization on Alginate Coated Sutures for the Prevention of Surgical Wound Infections and the *in vitro* Release Studies. International Journal of Nano Dimension (IJND, Winter), 2, 205-212.

Chaijareenont, P., Takahashi, H., Nishiyama, N., Arksornnukit, M. (2012) Effect of Different Amounts of 3-Methacryloxypropyltrimethoxysilane on the Flexural Properties and Wear Resistance of Alumina Reinforced PMMA. Dental Materials Journal, 31, 623-628.

Cooksey, K. (2005) Effectiveness of Antimicrobial Food Packaging Materials. Food Additives and Contaminants, 22, 980-987.

El-Kheshen, A. A., Gad El-Rab, S.F. (2012) Effect of reducing and protecting agents on size of silver nanoparticles and their anti-bacterial activity. Der Pharma Chemica, 4, 53-65.

Ghosh, B., Ramamoorthy, D. (2010) Effects of Silver Nanoparticles on *Escherichia Coli* and It's implications. International Journal of Chemical Science. 2010, 8, S31-S40.

Giri, A., Makhal, A., Ghosh, B., Raychaudhuri, A. K., Pal, S. K. (2010) Bio–Nanomaterials: Understanding Key Biophysics and Their Applications. Nanoscale, 2, 2704-2709.

Gorup, L.F., Longo, E., Leite, E.R., Camargo E.R. (2011) Moderating Effect of Ammonia on Particle Growth and Stability of Quasi-Monodisperse Silver Nanoparticles Synthesized by the Turkevich Method. Journal of Colloid and Interface Science, 360, 355-358.

Lamsal, K., Kim, S.W., Jung, J.H., Kim, Y.S., Kim, K.S., Lee, Y.S. (2011) Application of Silver Nanoparticles for the Control of *Colletotrichum* Species *In Vitro* and Pepper Anthracnose Disease in Field. The Koren Society of Mycology, 3, 194-199.

Maria, A. D., Aurora, A., Montone, A., Tapfer, L., Pesce, E., Balboni, R., Schwarz, M., Borriello, C. (2011) Synthesis and Characterization of PMMA/Silylated MMTs. Journal of Nanoparticle Research, 13, 6049-6058.

Marquez, M., Grady, B. P., Robb, I. (2005) Different Methods for Surface Modification of Hydrophilic Particulates with Polymers. Colloids and Surfaces A: Physicochemical and Engineering Aspects, 266, 18-31.

Nasrollahi, A., Pourshamsian, Kh., Mansourkiaee, P. (2011) Antifungal Activity of Silver Nanoparticles on Some of Fungi. International Journal of Nano Dimension (IJND), 3, 233-239.

Rodriguez, M. A., Liso, M. J., Rubio, F., Rubio, J., Oteo, J. L. (1999) Study of the Reaction of Gamma-Methacryloxypropyltrimethoxysilane (Gamma-MPS) with Slate Surfaces. Journal of Materials Science, 34, 3867-3873.

Shameli, K., Ahmad, M.B., Zargar, M., Yunus, W.M.Z.W., Ibrahim, N.A., Shabanzadeh, P., Moghaddam, M.G. (2011) Synthesis and Characterization of Silver/Montmorillonite/Chitosan Bionanocomposites by Chemical Reduction Method and Their Antibacterial Activity. International Journal of Nanomedicine, 6, 271-284.

Shameli, K., Ahmad, M.B., Yunus, W.M.Z.W., Ibrahim, N.A., Gharayebi, Y., Sedaghat, S. (2010) Synthesis of Silver/Montmorillonite Nanocomposites Using γ-Irradiation. International Journal of Nanomedicine, 5, 1067-1077.

Zhirong, L., Uddin, M. A., Zhanxue, S. (2011) FT-IR and XRD Analysis of Natural Na-Bentonite and Cu(II)-Loaded Na-Bentonite. Spectrochimica *Acta* Part A: Molecular and Biomolecular Spectroscopy, 79, 1013–1016.

Żymankowska-Kumon, S., Holtzer, M., Olejnik, E., Bobrowski, A. (2012) Influence of the Changes of the Structure of Foundry Bentonites on Their Binding Properties. Materials Science, 18, 57-61.